PNAS RESEARCH ARTICLE | NEUROSCIENCE

Repair of surviving hair cells in the damaged mouse utricle

Grace S. Kim[a], Tian Wang[a], Zahra N. Sayyid[a], Jessica Fuhriman[a], Sherri M. Jones[b], and Alan G. Cheng[a,1]

Edited by Ulrich Mueller, Johns Hopkins University, Baltimore, MD; received September 15, 2021; accepted February 21, 2022 by Editorial Board Member Jeremy Nathans

Sensory hair cells (HCs) in the utricle are mechanoreceptors required to detect linear acceleration. After damage, the mammalian utricle partially restores the HC population and organ function, although regenerated HCs are primarily type II and immature. Whether native, surviving HCs can repair and contribute to this recovery is unclear. Here, we generated the *Pou4f3*$^{DTR/+}$; *Atoh1*$^{CreERTM/+}$; *Rosa26R*$^{tdTomato/+}$ mouse to fate map HCs prior to ablation. After HC ablation, vestibular evoked potentials were abolished in all animals, with ∼57% later recovering responses. Relative to nonrecovery mice, recovery animals harbored more Atoh1-tdTomato^{+} surviving HCs. In both groups, surviving HCs displayed markers of both type I and type II subtypes and afferent synapses, despite distorted lamination and morphology. Surviving type II HCs remained innervated in both groups, whereas surviving type I HCs first lacked and later regained calyces in the recovery, but not the nonrecovery, group. Finally, surviving HCs initially displayed immature and subsequently mature-appearing bundles in the recovery group. These results demonstrate that surviving HCs are capable of self-repair and may contribute to the recovery of vestibular function.

hair cell | regeneration | repair | vestibular | utricle

Significance

The mammalian utricle shows limited hair cell regeneration despite partial recovery of function. Recovery of vestibular evoked potentials, a measure of utricular function, occurs after utricular hair cell damage in mammals. While previous work has shown limited regeneration in response to damage, most regenerating hair cells are type II with immature-appearing bundles. Whether hair cells that remain ("surviving hair cells") can self-repair and contribute to functional recovery is unknown. Using lineage tracing, we have characterized surviving hair cells over time and found that they repair bundles, regain innervation, and remain differentiated, and are therefore poised to contribute to the recovery of organ function.

Sensory hair cells are mechanoreceptors required for auditory and vestibular functions. They detect the mechanical signals of sound and head motion with exquisite sensitivity and in turn stimulate cochlear and vestibular afferents, which relay signals centrally for perception of these sensory inputs (1, 2). In mammals, cochlear hair cell loss is irreversible, resulting in permanent hearing loss (3). The utricle, a vestibular organ that detects linear acceleration, displays limited, spontaneous hair cell regeneration after damage in several mammalian species (4–12), with independent studies reporting a partial recovery of organ function (11–13).

In the human utricle, several pathologic conditions cause partial hair cell loss with many hair cells surviving presumably for years (14, 15). After acoustic trauma in vivo, both avian and mammalian cochlear hair cells have been shown to survive despite disrupted tiplinks and bundles (16). While avian cochlear hair cells repair and regenerate tiplinks and bundles in vitro (17) and in vivo (18), their mammalian counterparts only regenerate tiplinks but not bundles in vitro (19), suggesting that mammalian cochlear hair cells are less capable of repairing sublethal damage than avian hair cells. In the bullfrog saccule, hair cells damaged by the aminoglycoside gentamicin can survive as bundleless cells and undergo self-repair in vitro (20). Another study on the gerbil utricle reported that hair cells similarly repair bundles after gentamicin damage in vitro (21). However, there is a paucity of knowledge of to what extent mammalian vestibular hair cells can survive and self-repair after damage in vivo.

The utricle is composed of hair cells and supporting cells, with the former consisting of type I and type II subtypes distinguished by morphology, molecular markers, electrophysiological properties, and innervation (22–25). As a measure of utricular function, vestibular evoked potential (VsEP) responses are compound action potentials presumably resulting from activation of irregular afferents like those innervating type I hair cells in the central striolar region, as mutants without hair bundles or the striolar domain lack VsEP responses (26–28). After hair cell ablation, recovery of VsEP responses has been observed in neonatal and adult mouse utricles, even though regenerating hair cells primarily occupy the extrastriolar region and display mainly type II characteristics with immature-appearing stereociliary bundles (5, 7, 11, 12, 29, 30). At present, whether the recovery of VsEP responses can be fully attributed to regenerated hair cells or whether surviving hair cells also contribute is not clear.

Here we generated the *Pou4f3*$^{DTR/+}$; *Atoh1*$^{CreERTM/+}$; *Rosa26R*$^{tdTomato/+}$ mouse to concurrently ablate and fate map hair cells in the mouse utricle in vivo. After diphtheria toxin (DT) and tamoxifen administration, ∼83.5% of hair cells were ablated, and Atoh1-tdTomato marked surviving hair cells consisting of both type I and type II hair

Author affiliations: [a]Department of Otolaryngology–Head and Neck Surgery, Stanford University School of Medicine, Stanford, CA 94305; and [b]Department of Special Education and Communication Disorders, College of Education and Human Sciences, University of Nebraska, Lincoln, NE 68583

Author contributions: G.S.K. and A.G.C. designed research; G.S.K., T.W., Z.N.S., and J.F. performed research; G.S.K., T.W., Z.N.S., S.M.J., and A.G.C. analyzed data; and G.S.K., S.M.J., and A.G.C. wrote the paper.

The authors declare no competing interest.

This article is a PNAS Direct Submission. U.M. is a guest editor invited by the Editorial Board.

[1]To whom correspondence may be addressed. Email: aglcheng@stanford.edu.

This article contains supporting information online at http://www.pnas.org/lookup/suppl/doi:10.1073/pnas.2116973119/-/DCSupplemental.

Published April 5, 2022.

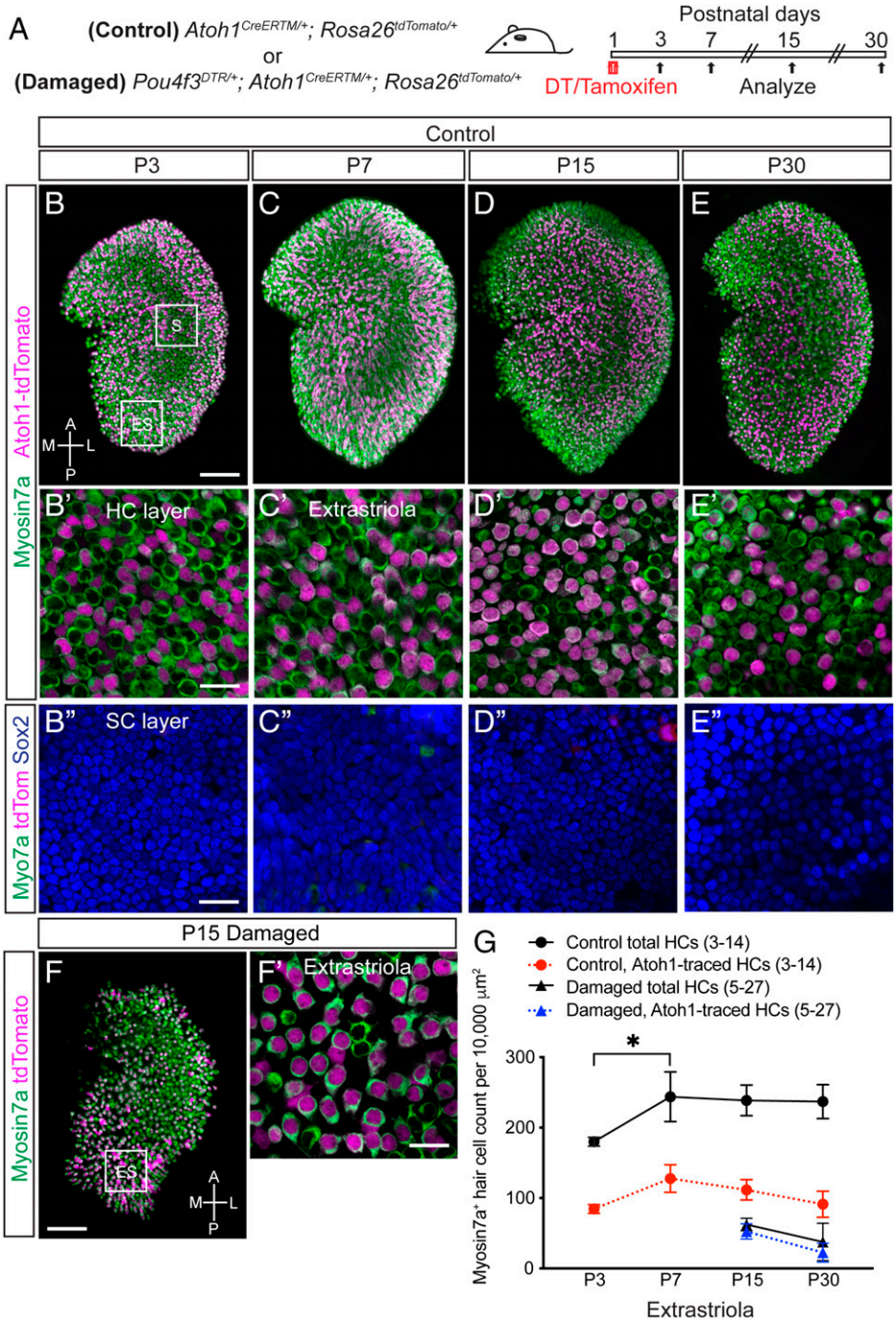

Fig. 1. Fate mapping hair cells in the damaged mouse utricle. (*A*) Schematic showing *Atoh1*$^{CreERTM/+}$*; Rosa26R*$^{tdTomato/+}$ (control, n = 3 to 14 mice) and *Pou4f3*$^{DTR/+}$*; Atoh1*$^{CreERTM/+}$*; Rosa26R*$^{tdTomato/+}$ (damaged, n = 5 to 27) mice treated with tamoxifen and DT at P1 to fate map and damage hair cells. Organs were examined at P3 to P30. (*B–E‴*) Fate-mapped Atoh1-tdTomato$^+$/Myosin7a$^+$ hair cells were detected throughout the utricle from P3 to P30. Representative high-magnification images from the extrastriolar region, showing many traced hair cells and rare traced supporting cells (SCs). HC, hair cell. (*F* and *F′*) After DT treatment at P1, both the size of the sensory epithelium and hair cell density in the extrastriola decreased at P15. (*G*) Quantification of the total and traced hair cell densities in the extrastriola of undamaged (control) and damaged utricles. Hair cell density in the extrastriolar region significantly increased between P3 and P7, and then remained mostly unchanged through P30. Density of traced hair cells in control utricles did not significantly change between P3 and P30. Relative to age-matched controls, density of total hair cells and traced hair cells of damaged utricles is significantly lower. A, anterior; L, lateral; M, medial; P, posterior. Data are shown as mean ± SD. One-way ANOVA. *$P < 0.05$. (Scale bars, 100 µm [*B–F*] and 20 µm [*B′–F′*].)

cells. All DT-injected animals lost VsEP responses 2 wk postablation, with ∼57% partially recovering VsEP responses 1 mo postdamage. By segregating animals into those that recovered VsEP responses and those that did not, we found that the recovery group contained significantly more surviving hair cells, composed of both type I and type II hair cells with characteristic molecular markers and innervation patterns. Significantly more surviving hair cells in the recovery than the nonrecovery group displayed calyceal innervation and synaptic colocalization, suggesting surviving hair cells recovered neural integration. Lastly, surviving hair cells in the recovery group exhibited significantly more mature-appearing, long stereociliary bundles than those in the nonrecovery group. Together, these results demonstrate that surviving hair cells both retain and repair functional components and may contribute to the recovery of vestibular function.

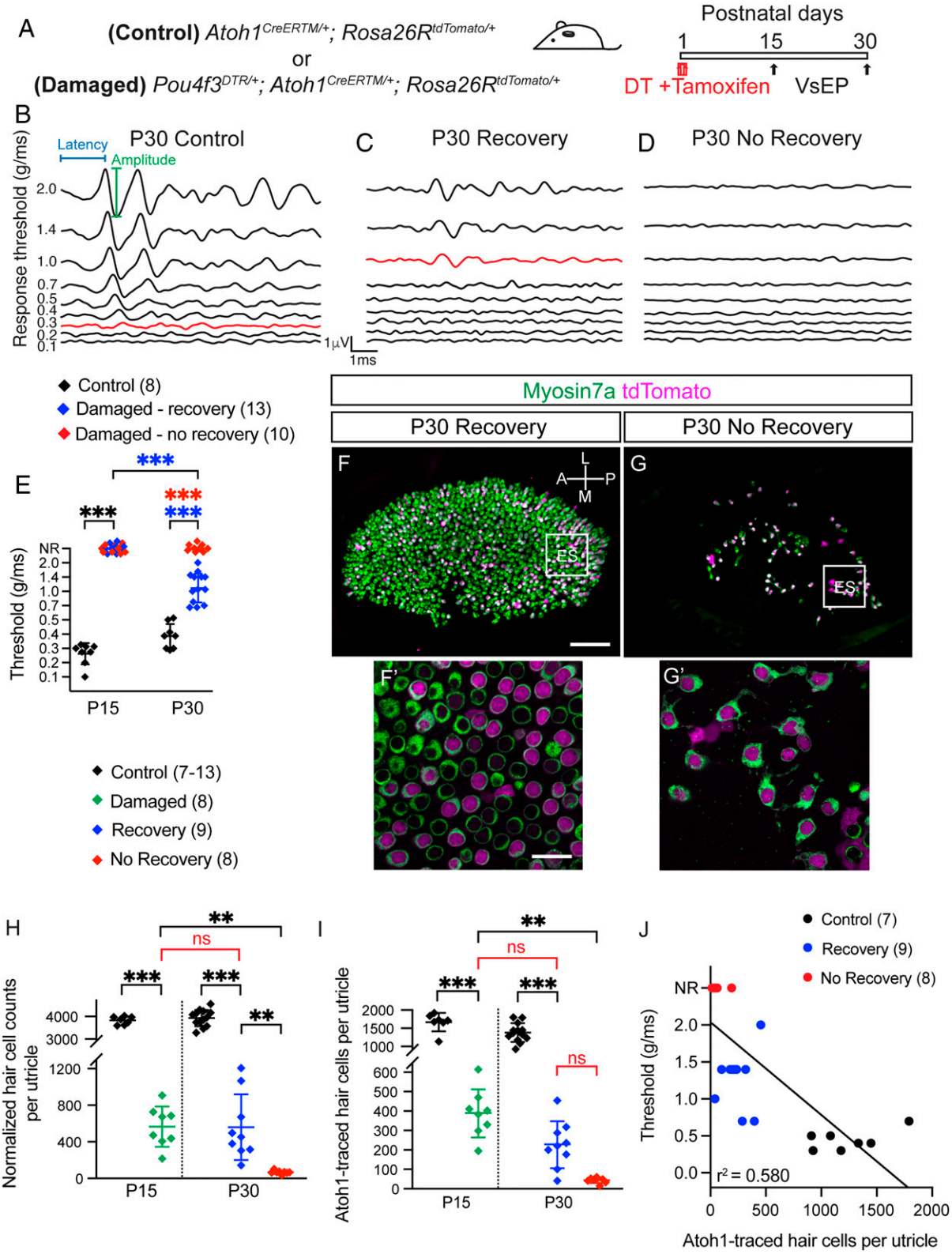

Fig. 2. Partial recovery of vestibular function after hair cell ablation. (*A*) Schematic of the experimental paradigm. *Atoh1*$^{CreERTM/+}$; *Rosa26R*$^{tdTomato/+}$ (control) and *Pou4f3*$^{DTR/+}$; *Atoh1*$^{CreERTM/+}$; *Rosa26R*$^{tdTomato/+}$ (damaged) mice were treated with DT and tamoxifen at P1 and examined at P15 and P30. (*B–D*) Representative VsEP tracings of a P30 control animal ($n = 8$) (*B*), a DT-injected P30 mouse with an initial loss of VsEP response at P15 and subsequent recovery ($n = 13$) (*C*), and a DT-injected P30 mouse with an initial loss of VsEP response at P15 and no subsequent recovery ($n = 10$) (*D*). (*E*) Scatterplots of VsEP thresholds of control and damaged animals. No damaged animals showed detectable VsEP response at P15. At P30, 57% of the damaged animals displayed VsEP thresholds, while 43% showed no response. (*F* and *F′*) Representative images of a utricle from a P30 recovery animal. (*G* and *G′*) Representative images of a utricle from a P30 nonrecovery animal, showing fewer hair cells compared with recovery animals. (*H*) Hair cell counts were significantly lower in the damaged P15 utricles than age-matched controls. The P30 recovery group hair cell counts were not significantly different from the P15 damaged group but were significantly higher than the P30 nonrecovery group ($n = 4$ to 13 mice). (*I*) There were significantly fewer Atoh1-traced hair cells in the damaged P15 utricles relative to controls. At P30, both the recovery and nonrecovery groups showed significantly fewer traced hair cells relative to the damaged P15 utricle ($n = 4$ to 13 mice). (*J*) The number of surviving Atoh1$^+$ hair cells per utricle correlated with their respective VsEP thresholds ($r^2 = 0.580$). NR, nonrecovery. Data are shown as mean ± SD. ES, extrastriola. One-way ANOVA. *$P < 0.05$, **$P < 0.01$, ***$P < 0.001$; ns, not significant. (Scale bars, 100 μm [*F* and *G*] and 20 μm [*F′* and *G′*].)

Results

Fate Mapping Surviving Hair Cells after Damage. The mouse utricle harbors over 2,000 hair cells at birth with additional hair cells added mainly in the first postnatal week (4). To label a subset of hair cells present at birth, we fate mapped hair cells in *Atoh1*$^{CreERTM/+}$; *Rosa26R*$^{tdTomato/+}$ (*Atoh1-Tomato*) mice (31, 32). After tamoxifen (0.075 mg/g intraperitoneally) was administered on postnatal day (P) 1 (Fig. 1*A*), we found that a subset of hair cells in both the extrastriola (84.6 ± 6.3 at P3 to 127.8 ± 19.4 at P30 per 10,000 μm^2, respectively, $n = 3$ to 14 mice; Fig. 1 *B*–*E*) and striola (53.3 ± 25.6 at P3 to 83.5 ± 7.8 at P30 per 10,000 μm^2, respectively, $n = 3$ to 14 mice; *SI Appendix*, Fig. S1 *A*–*D*) were tdTomato-labeled from P3 to P30. Supporting cells were rarely labeled (0 to 1 per 10,000 μm^2, $n = 28$ mice) in the extrastriola (Fig. 1 *B*″–*E*″) and striola (*SI Appendix*, Fig. S1 *A*′–*D*′) of all the utricles examined across each time point, indicating that fate mapping was highly specific to hair cells. On average, 44.0% of hair cells were tdTomato-labeled at P3, 49.1% at P7, 43.4% at P15, and 33.3% at P30 (Fig. 1*G* and *SI Appendix*, Fig. S1). As expected, an initial increase in hair cell counts was observed between P3 and P7 (Fig. 1*G* and *SI Appendix*, Fig. S1*F*), consistent with hair cell addition in the early postnatal period (33). Therefore, we attribute the decrease in percentage of tdTomato-labeled hair cells to the postnatal addition of unlabeled hair cells.

To selectively ablate hair cells, we used *Pou4f3*$^{DTR/+}$ mice, where the hair cell promoter Pou4f3 drives expression of the human diphtheria toxin receptor (DTR) (34). We generated *Pou4f3*$^{DTR/+}$; *Atoh1*$^{CreERTM/+}$; *Rosa26R*$^{tdTomato/+}$ (*DTR-Atoh1-Tomato*) mice to track surviving hair cells after damage. Tamoxifen and DT (4 ng/g, intramuscularly) were sequentially administered at P1 to label and ablate hair cells, respectively (Fig. 1*A*). After damage, there was a decrease in the overall size of the sensory epithelia (190,602.2 ± 4,670.6 μm^2 in control vs. 88,094.4 ± 17,139.5 μm^2 in damaged organs, $n = 5$ to 9 mice; *SI Appendix*, Table S1) as well as hair cell loss at P15 (Fig. 1 *F* and *F*′). Relative to age-matched, undamaged controls, there was a 73.9% decrease in hair cell density in the extrastriola (238.8 ± 21.7 per 10,000 μm^2, $n = 9$ control mice and 62.4 ± 8.8 per 10,000 μm^2, $n = 5$ DTR mice; Fig. 1*G*) and 66.5% in the striola (192.0 ± 37.0 per 10,000 μm^2, $n = 9$ control mice and 64.4 ± 10.3 per 10,000 μm^2, $n = 5$ DTR mice; *SI Appendix*, Fig. S1*F*) of the damaged P15 utricle. These results are consistent with previous studies (9, 11). In parallel, 47% of Atoh1-traced hair cells remained in both the extrastriola (111.7 ± 14.5 per 10,000 μm^2 to 52.6 ± 10.7 per 10,000 μm^2; Fig. 1*G*) and striola (76.9 ± 24.5 per 10,000 μm^2 to 37.2 ± 8.9 per 10,000 μm^2; *SI Appendix*, Fig. S1*F*) of the damaged P15 utricle, indicating that surviving hair cells were effectively labeled with this approach. Since Atoh1-Cre$^+$ hair cells were labeled prior to degeneration, Atoh1-tdTomato–labeled hair cells were deemed surviving hair cells hereon.

Hair Cell Ablation Causes Loss of Vestibular Function followed by a Partial Recovery. The neonatal mouse utricle can partially regenerate lost hair cells and recover organ function (4, 9, 11). Fate-mapping experiments have shown that most regenerating hair cells displayed immature bundles despite the recovery of organ function (11), leading us to hypothesize that surviving hair cells may contribute to this functional recovery. To test this hypothesis, we assessed utricular function after hair cell ablation by measuring VsEPs, which represent compound action potentials of the vestibular nerve and central relays as a result of a transient linear acceleration applied along the nasooccipital axis (35).

VsEP responses were blindly analyzed for *Atoh1-Tomato* control mice and *DTR-Atoh1-Tomato* damaged mice at P15 and P30 (Fig. 2*A*). Control P15 mice uniformly displayed robust VsEP thresholds (0.26 ± 0.07 g/ms, $n = 8$; Fig. 2*E*), latencies (1.59 ± 0.06 ms; *SI Appendix*, Fig. S2*A*), and amplitudes (2.78 ± 0.99 μV; *SI Appendix*, Fig. S2*B*). We examined 23 damaged mice at P15 (DT at P1) and found none with detectable VsEP responses (Fig. 2*E* and *SI Appendix*, Fig. S2 *A* and *B*).

Thirteen of the 23 damaged mice (57%) regained thresholds at P30 with an average response threshold of 1.19 ± 0.38 g/ms, while the remaining 10 mice showed no detectable thresholds (Fig. 2 *C*–*E*). To begin to investigate possible mechanisms underlying recovery of vestibular function, we separated animals that regained VsEP responses at P30 (recovery cohort) from those that did not (nonrecovery cohort). The P30 recovery animals displayed significantly higher thresholds (1.19 ± 0.38 g/ms, $n = 13$ mice, $P < 0.001$; Fig. 2 *C* and *E*) than age-matched, control mice (0.39 ± 0.15 g/ms, $n = 8$ mice; Fig. 2 *B* and *E*), corresponding to an incomplete functional recovery. The latency and amplitude of the VsEP recording for the recovery cohort were 2.12 ± 0.69 ms and 0.52 ± 0.32 μV ($n = 12$ mice), respectively, which were significantly longer and smaller than those of age-matched controls (1.58 ± 0.07 ms and 1.32 ± 0.54 μV, respectively, $n = 8$ mice, $P < 0.001$ for both; *SI Appendix*, Fig. S2 *A* and *B*). While these data agree with previous work demonstrating that a subset of animals recover VsEP responses (11), whether utricular histology differs between recovery and nonrecovery animals is unknown and is examined next.

Hair Cell Survival during Recovery of Utricular Function. Prior studies on the regenerating mammalian utricle showed that both the neonatal and adult organs are capable of partially replacing lost hair cells (11, 12). After DT-induced hair cell ablation, the P15 *DTR-Atoh1-Tomato* utricle displayed 85.2% fewer total hair cells (565.4 ± 220.7 per utricle, $n = 8$ mice) than age-matched, undamaged controls (3,826.3 ± 177.3 per utricle, $n = 7$ mice) (Fig. 2*H*). Similarly, there were significantly fewer tdTomato-labeled hair cells in the damaged P15 utricle (388.1 ± 123.8, $n = 8$ mice) compared with those in controls (1,665.4 ± 253.1, $n = 7$ mice, $P < 0.001$; Fig. 2*I*). However, labeled hair cells constituted 68.6% of all hair cells present after damage at P15, indicating most hair cells at this age were surviving hair cells.

At P15, hair cell counts in all the damaged utricles examined were remarkably similar, and there were no outliers to predict recovery and nonrecovery. However, when we separated P30 utricles into recovery and nonrecovery mice based on VsEP thresholds, we found that the former had a larger sensory epithelium (84,815.5 ± 26,305.3 μm^2 in recovery and 48,010.6 ± 17,446.1 μm^2 in nonrecovery, $n = 8$ or 9 mice) with significantly more hair cells compared with nonrecovery utricles (Fig. 2 *F*–*G*′). Hair cell counts per utricle in the P30 recovery group (559.8 ± 359.6, $n = 9$ mice; Fig. 2*J*) were significantly higher than the P30 nonrecovery cohort (67.0 ± 19.3, $n = 8$ mice, $P < 0.01$; Fig. 2*H*), with both significantly lower than age-matched controls (3,927.6 ± 363.1 hair cells, $n = 13$ mice, $P < 0.001$ for both; Fig. 2*H*). We also found a significant correlation between total hair cell counts and VsEP thresholds among control, recovery, and nonrecovery cohorts ($r^2 = 0.621$; *SI Appendix*, Fig. S2*C*). There was also no progressive hair cell loss from P15 damaged to P30 recovery, whereas the P30 nonrecovery displayed significantly lower hair cell counts than the

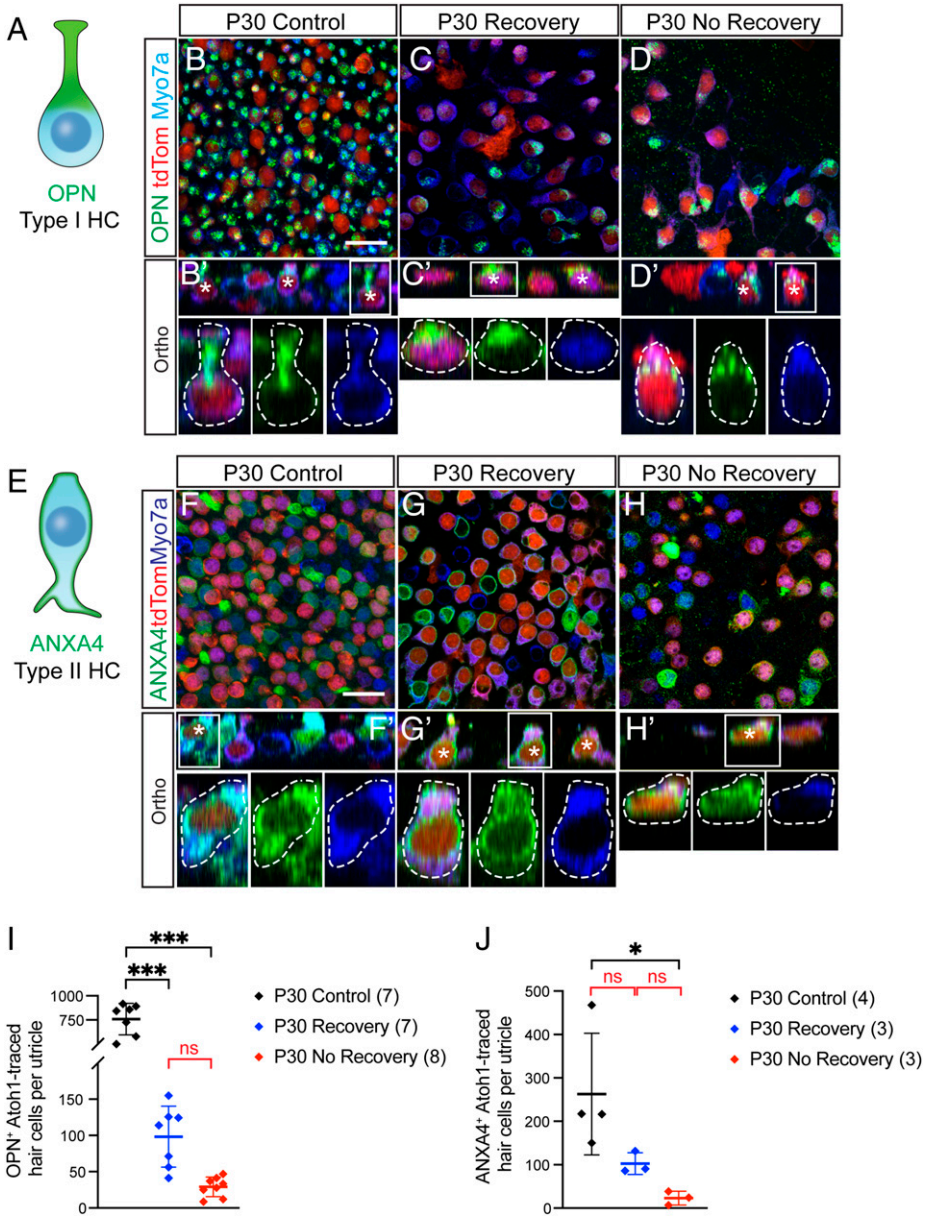

Fig. 3. Surviving hair cells express markers of type I and type II hair cells. (*A*) Cartoon depicting an amphora-shaped, OPN-positive type I hair cell with a long, thin apical neck. (*B* and *B*′) Many Atoh1-traced hair cells in the control *Atoh1*$^{CreERTM/+}$; *Rosa26R*$^{tdTomato/+}$ utricles expressed OPN in the apical neck region (asterisks). (*C*, *C*′, *D*, and *D*′) After damage-induced hair loss, a subset of Atoh1-traced, surviving hair cells in both the recovery and nonrecovery groups expressed OPN (asterisks). (*E*) Cartoon depicting an ANXA4-positive type II hair cell with a goblet-shaped cell body, a short thick neck, and basolateral cytoplasmic processes. (*F* and *F*′) Fate-mapped hair cells expressing ANXA4 in their cell membrane (asterisk) in the P30 control utricle. (*G*, *G*′, *H*, and *H*′) A subset of surviving hair cells displayed an ANXA4^{+} membrane (asterisks) in the recovery and nonrecovery groups. (*I* and *J*) Quantitative analyses showing fate mapped, surviving hair cells consist of both type I (OPN^{+}) and type II (ANXA4^{+}) hair cells, both significantly lower in the nonrecovery group ($n = 7$ or 8 mice for type I, 3 or 4 mice for type II). Data are shown as mean ± SD. One-way ANOVA. *$P < 0.05$, ***$P < 0.001$; ns, not significant. (Scale bars, 20 μm.)

P15 damaged utricle ($P < 0.05$; Fig. 2*H*). The lack of change in hair cell number from P15 damaged to P30 recovery can be attributed to the higher degree of damage achieved in this study compared with prior work (9, 11). Similarly, the number of traced, surviving hair cells was not significantly different between the P15 damaged and P30 recovery group (226.1 ± 121.1, $n = 9$ mice, $P = 0.40$; Fig. 2*I*) but significantly lower in the P30 nonrecovery group relative to the P15 damaged group (60.1 ± 51.1, $n = 6$ mice, $P < 0.01$; Fig. 2*I*). The number of traced, surviving hair cells also correlated with VsEP thresholds among control, recovery, and nonrecovery cohorts ($r^2 = 0.580$; Fig. 2*J*). While 89.7% of the hair cells in the P30 nonrecovery group were traced, only 40.4% were tdTomato-labeled in the recovery group (*SI Appendix*, Table S1), suggesting that the recovery organs consist of both surviving and regenerated hair cells while the nonrecovery organs contain mostly surviving hair cells. The number of untraced hair cells, which consist of both regenerated and surviving hair cells, also correlated with VsEP thresholds ($r^2 = 0.581$; *SI Appendix*, Fig. S2*D*), suggesting that regenerated hair cells may also contribute to functional recovery. Together, these results indicate that organs showing a recovery of function contained more total and surviving hair cells than those without recovery.

Surviving Hair Cells Maintain Both Type I and Type II Hair Cell Identities. Type I hair cells are characterized by amphora-shaped cell bodies and expression of osteopontin (OPN) in their thin, apical necks (23, 36). Within the sensory

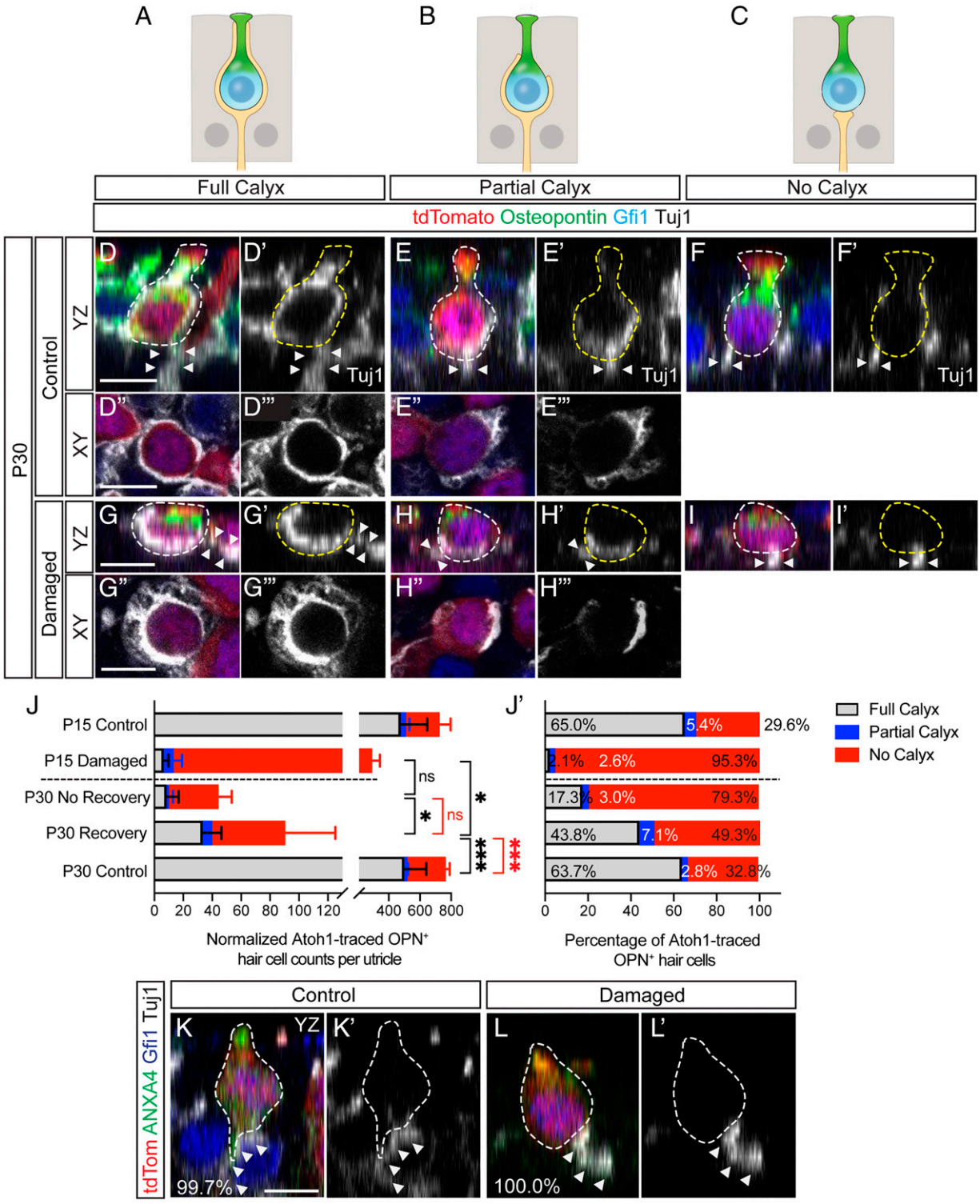

Fig. 4. Surviving type I and type II hair cells maintain and regain innervation. (*A–C*) Cartoons depicting type I hair cells with a full, partial, and no calyx. (*D–D‴* and *G–G‴*) Atoh1-traced, type I hair cells (dashed lines) with a full calyx are identified by Gfi1$^+$ nuclei, OPN$^+$ necks, and Tuj1$^+$ calyx (arrowheads) in P30 control *Atoh1*$^{CreERTM/+}$; *Rosa26R*$^{tdTomato/+}$ (*D–D‴*) and P30 damaged *Pou4f3*$^{DTR/+}$; *Atoh1*$^{CreERTM/+}$; *Rosa26R*$^{tdTomato/+}$ (*G–G‴*) utricles. Shown are orthogonal and *XY* views from *z*-stack images. (*E–E‴* and *H–H‴*) High-magnification images of OPN$^+$ type I hair cells (dashed lines) with a partial calyx (arrowhead along neurite) in P30 control (*E–E‴*) and P30 damaged (*H–H‴*) utricles. (*F*, *F*′, *I*, and *I*′) Some OPN$^+$ type I hair cells (dashed lines) had no calyx and only a bouton-like nerve terminal (arrowheads) abutting the cell in P30 control (*F* and *F*′) and P30 damaged (*I* and *I*′) utricles. (*J* and *J*′) Quantification of surviving type I hair cells with a full, partial, or no calyx showed a marked decrease in type I hair cells with full calyceal innervation and an increase in absent calyces in the damaged P15 utricles (n = 1,382 hair cells from 3 mice). Compared with P15 damaged utricles, there were significantly more hair cells with full calyces in the P30 recovery cohort (n = 540 hair cells from 4 mice). No significant change in full calyx counts in the P30 nonrecovery group (n = 433 hair cells from 6 mice) relative to P15 damaged utricles. This is reflected in the percentage of traced surviving hair cells with and without calyces in each group. A greater proportion of the surviving type I hair cells had a full calyx in the P30 recovery group compared with the P30 nonrecovery group, although this was still a smaller percentage compared with P30 controls. (*K* and *L*) ANXA4$^+$, Gfi1$^+$ type II hair cells (dashed lines) juxtaposed to a Tuj1$^+$ neurite (arrowheads) in P30 control (*K* and *K*′) and P30 damaged (*L* and *L*′) utricles. All ANXA4$^+$ surviving type II hair cells were adjacent to a Tuj1$^+$ neurite (n = 308 and 70 hair cells from 3 mice each for P30 control and P30 damaged, respectively). Data are shown as mean ± SD. One-way ANOVA. *P < 0.05, ***P < 0.001; ns, not significant. (Scale bars, 5 μm.)

epithelium, hair cell and supporting cell nuclei are laminated, with type I hair cell nuclei residing at a lower level than type II hair cell nuclei but above those of supporting cells (37). About 55% of Atoh1-traced hair cells in the P30 control utricle were amphora-shaped and displayed OPN$^+$ necks and nuclei at a level closer to the supporting cells, and were therefore determined to be type I (759.5 ± 163.1, $n = 7$ mice; Fig. 3 *A–B′* and *I*). After damage, the sensory epithelium was flattened with a loss of distinct layers, and hair cell subtypes could not be determined based on morphology or nucleus location. Traced type I hair cells in both the recovery and nonrecovery utricles still expressed OPN in their apical region but were pear-shaped, and they displayed neither an apical neck nor amphora shape (Fig. 3 *C–D′*), consistent with those previously reported findings (11). The number of OPN$^+$ traced hair cells in the P30 recovery utricles (98.3 ± 42.0, $n = 7$ mice; Fig. 3*I*) trended higher than the P30 nonrecovery utricles (27.8 ± 13.5, $n = 8$ mice, $P = 0.57$; Fig. 3*I*), corresponding to about 45% of surviving hair cells being type I in both groups (*SI Appendix*, Table S1).

Type II hair cells are morphologically characterized by their goblet shape, short, thick necks, basolateral cytoplasmic projections, and expression of SOX2 and AnnexinA4 (ANXA4) (11, 12, 23, 37). In the P30 control, *Atoh1-tdTomato* utricles, we found that 262.9 ± 140.0 traced hair cells ($n = 4$ mice; Fig. 3*J*) displayed basolateral processes and expressed a membranous pattern of ANXA4, and were therefore determined to be type II (Fig. 3 *E–F′*). After damage, Atoh1-tdTomato–labeled hair cells expressing ANXA4 appeared short and lacked a distinct neck region. The thickness of the sensory epithelium and therefore the height of the cells varied across the mice after damage, findings consistent with those previously reported (11). The number of traced type II hair cells in the P30 recovery (102.7 ± 25.1, $n = 3$ mice; Fig. 3 *G*, *G′*, and *J*) trended higher relative to the nonrecovery utricles (23.2 ± 15.9, $n = 3$ mice, $P = 0.57$; Fig. 3 *H*, *H′*, and *J*), with about 40% of surviving hair cells found to be type II in both groups (*SI Appendix*, Table S1).

Overall, both P30 recovery and nonrecovery groups contained surviving hair cells with characteristics of type I and type II hair cells, albeit fewer of each subtype than age-matched controls ($P < 0.05$ for both; Fig. 3 *I* and *J*) given the overall decrease in the number of hair cells after damage.

Surviving Hair Cells Remain Neurally Integrated. Type I and type II hair cells have distinct innervation patterns, with the former encased in calyceal afferent fibers and the latter abutted by boutons (38). To determine if surviving hair cells remained neurally integrated, we first immunostained for Tuj1$^+$ neurites in the undamaged *Atoh1-tdTomato* utricle.

As type I hair cells mature during the first postnatal month, they can be categorized by their calyx being full (Fig. 4 *A* and *D–D′′*), partial (Fig. 4 *B* and *E–E′′*), or absent (Fig. 4 *C*, *F*, and *F′*) (38, 39). A full calyx encircles at least 95% of the cell body and reaches the neck region, while a partial calyx encases less than 95% and/or does not reach the neck region. In the P15 undamaged, *Atoh1-tdTomato* utricle, most traced OPN$^+$ type I hair cells displayed full calyces (475.2 ± 170.4, 65.6%, $n = 4{,}727$ hair cells from 3 mice; Fig. 4 *J* and *J′* and *SI Appendix*, Table S1) with 34.4% showing partial or no calyces (34.1 ± 23.7 with partial calyx and 214.6 ± 72.9 with no calyx, $n = 3$ mice; Fig. 4 *J* and *J′* and *SI Appendix*, Table S1). Damage led to significantly fewer traced OPN$^+$ type I hair cells with full calyces in the P15 *DTR-Atoh1-Tomato* utricle (2.2%, 6.3 ± 3.5 per utricle, $n = 1{,}382$ hair cells from 3 mice, $P < 0.001$; Fig. 4 *J* and *J′*), with almost all type I hair cells lacking calyces (95.5%, 278 ± 51.2, $n = 3$ mice; Fig. 4 *J* and *J′*).

Relative to the damaged P15 utricle, there were five times more surviving type I hair cells with full calyces in the P30 recovery group (33.2 ± 13.2, $n = 540$ hair cells from 4 mice, $P < 0.05$), whereas it was not significantly different in the P30 nonrecovery group (8.3 ± 8.5, $n = 433$ hair cells from 6 mice, $P = 0.63$) (Fig. 4 *G–G′′*, *J*, and *J′*). These data corresponded to more surviving type I hair cells with full calyces (36.8%) in the P30 recovery mice than the P30 nonrecovery group (25.7%, $P < 0.05$; Fig. 4 *J* and *J′* and *SI Appendix*, Table S1), with both groups containing fewer than the age-matched controls (497.7 ± 143.4, $n = 3{,}629$ hair cells from 4 mice, $P < 0.001$; Fig. 4 *J* and *J′*).

Conversely, surviving hair cells with no calyces decreased in the recovery group but remained high in the nonrecovery group (55.1%, 49.7 ± 36.1, $n = 4$ mice and 77.1% had no calyx, 34.0 ± 9.4, $n = 6$ mice, respectively; Fig. 4 *J* and *J′* and *SI Appendix*, Table S1). Surviving hair cells with partial calyces were infrequent in both the recovery and nonrecovery groups (8.0%, 7.2 ± 6.0, $n = 4$ mice and 4.1%, 1.8 ± 2.8, $n = 6$ mice, respectively). Both had proportionally more partial or no calyces than the P30 undamaged, control utricles (2.8%, 21.3 ± 5.1, $n = 4$ mice and 32.1%, 244.8 ± 26.6, $n = 4$ mice, respectively; Fig. 4 *J* and *J′* and *SI Appendix*, Table S1). The number of OPN$^+$ surviving type I hair cells with partial and absent calyces was not significantly different between the P30 recovery and nonrecovery groups. Taken together, these results suggest that damage induced an initial loss of calyces among surviving type I hair cells, after which more surviving type I hair cells regained calyces in the recovery than nonrecovery group.

Tenascin-C (TnC) is an extracellular matrix protein in the type I hair cell–calyx junction in avian (40) and mammalian vestibular organs (41, 42). In the avian maculae, TnC has been implicated to mediate calyx formation and maintenance after damage (40). We immunostained for TnC in P15 and P30 control utricles and found that most OPN$^+$, traced type I hair cells with a full or partial Tuj1$^+$ calyx coexpressed TnC (69.7%, 355.3 ± 147.2 cells at P15 and 90.2%, 490.9 ± 76.8 cells at P30, $n = 4{,}727$ and 3,477 hair cells from 3 mice for both; *SI Appendix*, Fig. S3 *A–A′′*, *D–D′′*, and *E*). In the P15 damaged utricle, most TnC$^+$ type I hair cells lacked calyces (20.0 ± 18.3, 71.2%, $n = 1{,}382$ hair cells from 3 mice; *SI Appendix*, Fig. S3 *B–B′′* and *E* and Table S1). Relative to the P15 damaged utricle, the P30 recovery group, but not the nonrecovery group, contained more OPN$^+$/TnC$^+$ surviving type I hair cells with full calyces (*SI Appendix*, Fig. S3 *C–C′′* and *E* and Table S1). In the P30 recovery group, most OPN$^+$/TnC$^+$ surviving type I hair cells had full and partial calyceal junctions (84.5%, 31.5 ± 24.8 cells per utricle, $n = 128$ hair cells from 2 mice; *SI Appendix*, Fig. S3 *C–C′′* and *E* and Table S1), which was more than the P30 nonrecovery group (75.5%, 11.4 ± 16.2 hair cells per utricle, $n = 92$ hair cells from 2 mice; *SI Appendix*, Fig. S3*E*). Overall, our damage model captured an initial decline in TnC$^+$ surviving type I hair cells with calyces followed by a restoration of calyces in the recovery group, consistent with the concept that TnC mediates calyx formation.

Type II hair cells are innervated by bouton nerve terminals. In both the P15 control and damaged utricles, all ANXA4$^+$, Atoh1-traced type II hair cells were innervated by Tuj1$^+$ neurites. Similarly, in P30 control and damaged utricles, nearly all ANXA4$^+$, Atoh1-traced type II hair cells were also innervated

by Tuj1$^+$ neurites (99.7% in control, 100% in damaged; Fig. 4 *K* and *L*). All ANXA4$^+$, Atoh1-traced type II hair cells in both the P30 recovery ($n = 308$ hair cells from 3 mice) and nonrecovery groups ($n = 70$ hair cells from 3 mice) had Tuj1$^+$ boutons abutting the hair cell, suggesting that surviving type II hair cells remained innervated in both groups. Alternatively, they may have been temporarily denervated and later regained innervation.

To further examine the integrity of hair cell innervation, we immunostained for pre- and postsynaptic elements of the Atoh1-traced surviving hair cells. Ctbp2 is a major component of the hair cell presynaptic ribbon while Homer1 is a postsynaptic density scaffold protein (43–45). Colocalization of pre- and postsynaptic proteins has been used as a proxy for functional, mature hair cell synapses (38). In the P15 control utricle, there were 3.3 ± 1.6 colocalized synaptic proteins in the basolateral aspect of each traced type I hair cell and 7.2 ± 3.0 per traced type II hair cell, which were readily determined by their morphology and nucleus location ($n = 18$ type I and 18 type II hair cells from 6 mice; *SI Appendix*, Fig. S4*E*).

After damage, when hair cell morphology and lamination were distorted, we used ANXA4 labeling to distinguish type I (ANXA4-negative) and type II (ANXA4$^+$) surviving hair cells (*SI Appendix*, Fig. S4 *C–D″*). We found that both surviving type I and type II hair cells still displayed numerous colocalized synapses at P15 and P30 after damage. At P15, there was no significant difference in the number of paired synapses per surviving type I hair cell (6.5 ± 2.9, $n = 14$ hair cells from 4 mice, $P = 0.46$; *SI Appendix*, Fig. S4*E*) compared with age-matched controls. No significant difference was observed between P15 damaged mice and P30 recovery (5.6 ± 3.4, $n = 12$ hair cells from 5 mice, $P = 0.99$) or P30 nonrecovery mice (6.6 ± 7.8, $n = 21$ hair cells from 7 mice, $P = 0.96$) (*SI Appendix*, Fig. S4*E*). There was also no significant difference in paired synapse counts per surviving type I hair cell between P30 recovery and P30 nonrecovery mice ($P > 0.99$), nor when each was compared with P30 controls ($P = 0.47$ and $P = 0.53$, respectively).

In contrast, there was a significant change in synapses per surviving type II hair cell at P15 after damage (11.9 ± 3.2, $n = 13$ hair cells from 4 mice, $P < 0.01$; *SI Appendix*, Fig. S4*E*) compared with age-matched controls. While there was no significant change between P15 damaged and P30 recovery utricles, surviving type II hair cells of the P30 recovery mice had significantly more colocalized synapses (11.7 ± 3.4, $n = 14$ hair cells from 5 mice) than the P30 nonrecovery mice (7.8 ± 4.6, $n = 23$ hair cells from 7 mice, $P < 0.05$) and P30 control ($P < 0.001$) (*SI Appendix*, Fig. S4 *D–D″* and *E*). In fact, there was a significant decrease in the number of synapses per surviving type II hair cell from P15 damaged to P30 nonrecovery ($P < 0.05$; *SI Appendix*, Fig. S4*E*).

During recovery of hair cell synapses after noise damage, a reduction of orphan presynaptic ribbon proteins (e.g., Ctbp2$^+$ puncta without an adjacent Homer1$^+$ puncta) has been reported (46). No significant difference in the number of orphan ribbon proteins was identified in surviving type I and type II hair cells in the P30 control, recovery, or nonrecovery utricles (*SI Appendix*, Fig. S4*F*). Altogether, these data indicate that surviving type I and type II hair cells contain components of functional synapses after damage, with surviving type II hair cells showing an increase in the number of colocalized synapses in response to damage.

Overall, while there are fewer total hair cells and Atoh1-traced hair cells after damage, more surviving type I hair cells initially lacked and later regained full calyces in the P30 recovery group. All surviving type II hair cells remained innervated in the recovery and nonrecovery groups at both P15 and P30 after damage. In addition, surviving type I and type II hair cells maintained paired pre- and postsynapses, with the latter showing an increase in the P30 recovery group. Altogether, these results suggest that surviving hair cells are neurally integrated and may contribute to the recovery of organ function.

Surviving Hair Cells with Intact Hair Bundles in Organs Recovering Function. As mechanoreceptors, hair cells are crowned with bundles that are essential for organ function. Previously, regenerated hair cells displayed mostly short and immature-appearing bundles despite recovery of organ function (7, 11, 12). To assess bundles among traced surviving hair cells, we used fluorescence-conjugated phalloidin to mark Atoh1-traced hair cells from P15 and P30 utricles (Fig. 5 *A–E*) and assessed them based on established morphologic criteria (Fig. 5 *F–F′*) (7). After damage at P15, there were significantly fewer surviving hair cells with long bundles (6.5%, 18.6 ± 10.4, $n = 857$ hair cells from 3 mice; Fig. 5*B*) compared with age-matched controls (87.0%, 1,661.0 ± 280.2, $n = 5,730$ hair cells from 3 mice, $P < 0.001$) (Fig. 5 *A*, *G*, and *G′* and *SI Appendix*, Table S1). Strikingly, many surviving hair cells displayed short bundles or were bundleless (Fig. 5*B*), reminiscent of developing and regenerating hair cells (11). In contrast, many surviving hair cells in the P30 recovery group displayed long bundles (Fig. 5 *C* and *D*) whereas those in the P30 nonrecovery group showed short or no bundles (Fig. 5*E*). There were significantly more surviving hair cells with long bundles in the P30 recovery group (41.8%, 192.4 ± 54.0, $n = 1,225$ hair cells from 3 mice, $P < 0.05$) than the P15 damaged group or the P30 nonrecovery group (31.1%, 18.8 ± 16.4 hair cells, $n = 169$ hair cells from 3 mice, $P < 0.05$), although significantly fewer than P30 controls (85.0%, 1,457.9 ± 48.3, $n = 5,233$ hair cells from 3 mice, $P < 0.001$; Fig. 5 *G* and *G′* and *SI Appendix*, Table S1). These data suggest that surviving hair cells initially displayed nascent or no bundles, and later displayed more mature-appearing bundles during recovery of organ function.

To compare surviving with regenerated hair cells, we next examined *Pou4f3*$^{DTR/+}$; *Plp1*$^{CreERT/+}$; *Rosa26R*$^{tdTomato/+}$ (*DTR-Plp1-Tomato*) mice, where supporting cells were fate mapped (tamoxifen administered at P8) following DT-induced hair cell ablation at P1 (*SI Appendix*, Fig. S5*A*). This approach has been used to mark regenerated hair cells derived from a supporting cell population in the mouse utricle (11). All 10 damaged *DTR-Plp1-Tomato* mice lacked VsEP responses at P15, with 60% recovering thresholds at P30. As expected, both the P30 recovery and nonrecovery utricles contained fewer hair cells than age-matched controls (307.0 ± 280.0, 157.1 ± 83.1, and 3,836.6 ± 717.2 hair cells, respectively, from 4 to 7 mice; *SI Appendix*, Fig. S5 *B–D*). Both recovery and nonrecovery utricles displayed Plp1-tdTomato–labeled, regenerated hair cells (27.6 ± 30.0 and 14.0 ± 11.9 from 4 to 6 mice; *SI Appendix*, Fig. S5*E*). While the number of regenerated hair cells correlated with VsEP thresholds ($r^2 = 0.339$; *SI Appendix*, Fig. S5*F*), they merely represented 9.0 and 8.9% of the remaining hair cell populations in the recovery and nonrecovery groups, respectively.

Next, we compared bundle morphology between regenerated and surviving hair cells in the damaged utricle. In the P30 undamaged, control *Plp1-Tomato* utricles, almost all hair cells

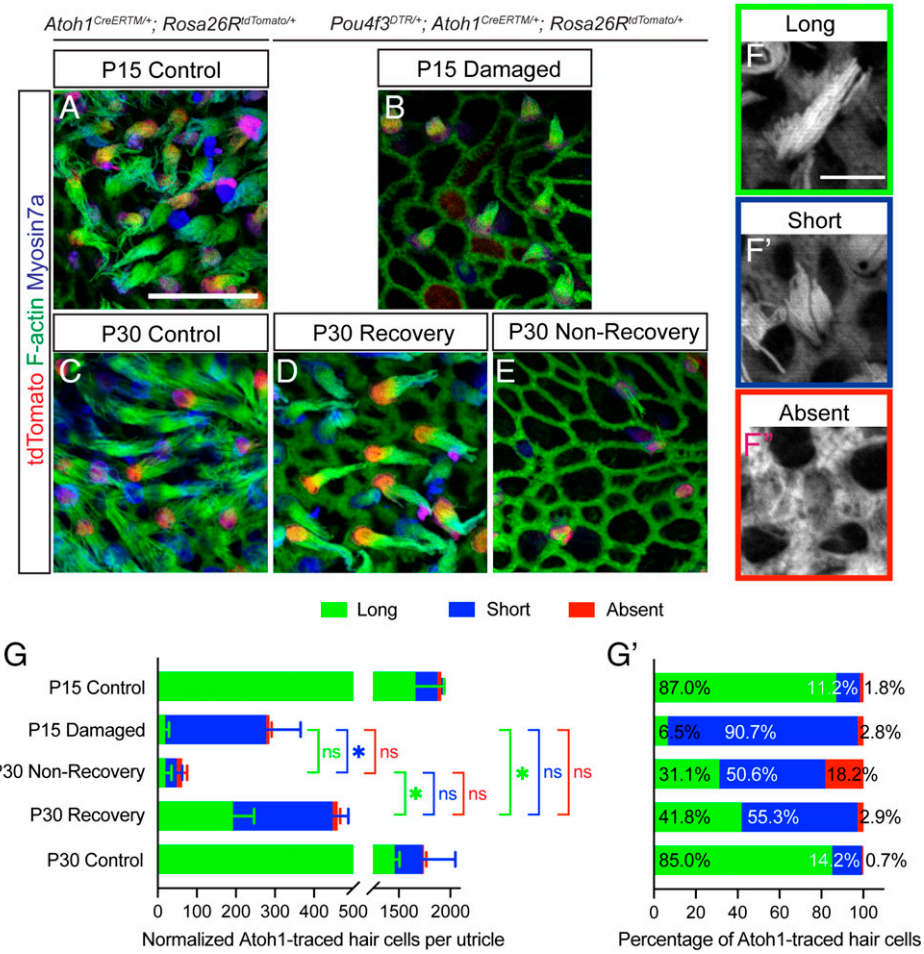

Fig. 5. Surviving hair cells repair stereociliary bundles. (*A–E*) High-magnification images of phalloidin-labeled bundles from control (*Atoh1*$^{CreERTM/+}$; *Rosa26R*$^{tdTomato/+}$) and damaged (*Pou4f3*$^{DTR/+}$; *Atoh1*$^{CreERTM/+}$; *Rosa26R*$^{tdTomato/+}$) utricles. At P15, most bundles of surviving hair cells appeared short after damage relative to controls. At P30, most bundles of surviving hair cells in the recovery group appeared elongated and comparable to controls, although fewer hair cells were present. The number of surviving hair cells was not significantly different between the P15 damaged and P30 recovery groups. Surviving hair cells in the P30 nonrecovery group were mostly bundleless or displayed short bundles, and were significantly fewer than the P15 damaged group. (*F–F″*) Representative high-magnification images of hair cells with long, short, or absent phalloidin-labeled bundles. (*G* and *G′*) Normalized counts and percentages of surviving hair cells with long, short, or no bundles. At P15, most (90.7%) bundles of surviving hair cells were short and 6.5% were long (n = 857 hair cells from 3 mice). At P30, the recovery group contained more surviving hair cells with long bundles relative to P15 damaged and the P30 nonrecovery group (n = 1,225 and 169 hair cells from 3 mice each for P30 recovery and nonrecovery, respectively). Data are shown as mean ± SD. One-way ANOVA. *$P < 0.05$; ns, not significant. (Scale bars, 20 μm [*A–E*] and 2 μm [*F–F″*].)

have long bundles (*SI Appendix*, Fig. S5*G*). In the P30 damaged *DTR-Plp1-Tomato* utricles, traced, regenerated hair cells displayed a mixture of long, short, and absent bundles (*SI Appendix*, Fig. S5*H*). Consistent with previous results, we found that most Plp1-tdTomato–traced, regenerated hair cells displayed short or no bundles and few had long bundles (79.1 and 14.0%, $n = 129$ cells from 5 mice; *SI Appendix*, Fig. S5 *I* and *I′*) (11). By contrast, most untraced hair cells had long bundles (73.9%, 105.5 ± 9.3 cells, $n = 617$ cells from 4 mice, $P < 0.001$; *SI Appendix*, Fig. S5 *I* and *I′*). As these untraced hair cells likely contain surviving hair cells, these results are consistent with the notion that most Atoh1-traced surviving hair cells displayed long bundles. Together, these results suggest that most surviving hair cells first displayed immature and subsequently mature-appearing bundles during recovery of organ function, implicating their ability to self-repair.

Discussion

While the loss of mammalian cochlear hair cells leads to permanent hearing loss, the mammalian utricle has the capacity to recover vestibular function (11, 12, 47). The mammalian utricle has shown limited spontaneous hair cell regeneration; however, the regenerated hair cells have immature-appearing bundles despite grossly normal synaptic elements and innervation (7, 11, 12), leaving open the possibility that surviving hair cells or other cellular components through repair may also contribute to the recovery of vestibular function.

Hair cells in the amphibian and mammalian vestibular systems have been shown to be capable of repairing damaged bundles (20, 21). Therefore, the functional recovery of the mammalian vestibular system is potentially attributed to both the regeneration of new hair cells and the repair of damaged hair cells. By tracing hair cells before damage, we have shown that surviving hair cells displayed markers of both hair cell subtypes, retained and regained neural integration, and regained long apical bundles, which were identified more commonly in the surviving hair cell population of organs that recovered function.

Bundle Integrity in Surviving Hair Cells. During mouse development, vestibular hair cells begin to form from neuroepithelial progenitors around embryonic age (E) 11.5 (48), and hair bundles are first detected around E13.5 (49, 50). Some hair cells

have long mature-appearing bundles at birth while others, including those added postnatally, appear short and immature. Previously, Gale and colleagues showed that there were bundleless hair cells in the bullfrog saccules that survived for at least 1 wk after aminoglycoside-induced damage (20). After 4 and 7 d of culture, they observed small, repairing hair bundles alongside larger surviving bundles, suggesting intracellular repair in the absence of mitosis (20). There is only one report that mammalian vestibular hair cell bundles were repaired after gentamicin damage in vitro (21). Here our data suggest that in this transgenic model, DT can cause sublethal damage to hair cells, which survive and first display nascent bundles and subsequently more mature-appearing bundles, suggesting bundle repair in mammalian vestibular hair cells in vivo.

In the mammalian utricle, both postnatally generated and regenerated hair cells have underdeveloped stereociliary bundles although some uptake of fluorescence-tagged aminoglycosides was detected, suggesting the presence of patent mechanoelectrical transduction channels (9, 11). Here, we observed that surviving hair cells from both recovery and nonrecovery groups shifted from mostly showing short to long bundles after damage between P15 and P30. While the recovery group had significantly more hair cells than the nonrecovery group overall, we hypothesize that there is a threshold of surviving hair cells with long bundles required for organ function. Thus, bundle length may be a proxy for the repair and integrity of surviving hair cells to determine the likelihood of recovery of organ function in the vestibular system. Whether these surviving hair cells are fully functional as mechanoreceptors remains unknown.

Recovery of Innervation and Synapses. During regeneration of avian vestibular hair cells, there is initially retraction of afferent fibers into the underlying stromal tissue (51–53) followed by neuronal growth cone extension (1 wk) and neuronal arborizations (2 to 4 wk) during recovery (53). Recovery of motion-evoked responses from vestibular afferent neurons has also been reported following regeneration of hair cells in avian cristae (54–56). While the pattern of neural retraction and regrowth has been extensively studied in regeneration, it is unclear how the innervation of surviving hair cells is altered if at all after damage.

In our study, we observed that the innervation patterns of type II hair cells were similar in recovery and nonrecovery utricles. However, there was a progressive loss of surviving type II hair cells in the nonrecovery utricles, resulting in fewer type II hair cells than the recovery group. It is possible that there exists a critical threshold of innervated type II hair cells and type I hair cells for the utricle to function.

On the other hand, damage led to calyceal loss in many type I hair cells at P15 and an emergence of type I hair cells with partial or no calyces. Partial calyces have previously been reported in the first 2 to 4 d of developing postnatal mouse utricles (38, 39) as well as in the chinchilla utricle after gentamicin-induced hair cell damage and loss of calyces (57). The presence of such partial calyces in our study may represent retracted neurites primed to recover and become full calyces.

TnC, an extracellular matrix protein, has been shown to be involved in cell migration, proliferation, differentiation, attachment and detachment, and as a homeostatic factor in tissue repair (58, 59). In particular, one study on spinal cord injury showed up-regulation of TnC expression in regenerating neurons promoting axonal growth and synapse formation (60). In the inner ear, TnC is found in the junction of type I hair cells and afferent calyces in avian (40) and mammalian vestibular organs (41, 42). Prior studies have shown the loss of TnC expression after ototoxic injury in chicken utricles with subsequent return of TnC-labeled hair cells and Tuj1-positive calyces upon regeneration (40). Similarly, we observed an increase in TnC-labeled surviving hair cells without calyces at P15 after damage, followed by a return of calyces by P30. These results suggest that surviving type I hair cells can gain calyx innervation after injury, possibly mediated by TnC; however, future work will be needed to further delineate this process and underlying mechanisms. Our fate-mapping model and these results should serve as the foundation for these future studies.

In the cochlea, previous work has shown a progressive loss of synapses after noise-induced trauma with eventual synaptic recovery and neural regeneration (46). In our model, we noted no apparent loss of colocalization of pre- and postsynaptic proteins in surviving hair cells. Instead, we detected an increase in colocalized synapses in surviving type II hair cells in the P30 recovery group. Whether this indicates a more generalized synaptic recovery after damage and its potential effects on organ function are unknown.

The threshold, latency, and amplitude of the waveforms represent the overall organ sensitivity, timing of neural transmission, and size and synchrony of the activated neuronal population, respectively (61). Functional hair cells are critical for VsEP responses as mutant mice with deficient stereociliary bundles or hair cell loss had elevated thresholds, prolonged latencies, and decreased amplitudes (26, 62). In addition, hair cell number appears to correlate with VsEP responses; however, no hair cell number threshold above which there is a consistent response has been identified (12). The overall number of hair cells, bundle morphology, and their neural integration (i.e., innervation and synapses) may account for the return of VsEP responses. We postulate that the presence of long apical bundles, afferent innervation with synapses particularly of type I hair cells, and a certain threshold number of hair cells likely improve neural transmission and synchronization.

Surviving versus Regenerated Hair Cells. Although regenerated vestibular hair cells display functional somatic features such as afferent innervation and synapses, they lack mature-appearing apical bundles (11). Given that and the limited number of spontaneously regenerated hair cells, it is unlikely that regeneration alone is responsible for functional recovery (11, 12). Other possible contributing factors include surviving hair cells that undergo repair. Similar to the previous studies, we observed only a limited degree of regeneration (~9% of hair cells traced) despite functional recovery in ~57% of damaged mice, implicating a potential role of surviving hair cells which made up 40% of the utricle during recovery of organ function. In support of this notion, we found a significant correlation between the number of surviving Atoh1$^+$ hair cells and VsEP thresholds.

Both regenerated and surviving hair cells in the recovery utricles appeared round and flat, thus requiring molecular markers instead of morphological features to distinguish hair cell subtypes. While 45% of surviving hair cells were type I with ~37% of which displaying with full calyces, 90% of regenerated hair cells have been reported to be type II with almost no regenerated hair cells showing calyces or OPN expression (11). Finally, more surviving than regenerated hair cells had long bundles (42 vs. 14%). Of note, we have previously observed more hair cells and animals recovering VsEP responses at P60, suggesting an increasing number of regenerated hair cells over time. While it is difficult to separate the contributions of surviving versus regenerated hair cells, it is

likely a concerted effect of both resulting in functional recovery. Transcriptomic analyses of the surviving hair cells and longer studies in the future should reveal mechanisms of repair to further delineate their roles during recovery of organ function.

In summary, we found that surviving hair cells in damaged utricles maintain subtype specialization, retain and regain innervation, and potentially repair bundles. Organs that recover function displayed more type I and type II hair cells that were innervated and had mature-appearing stereociliary bundles. Repair of surviving hair cells, both spontaneous and therapeutically activated, may serve as an alternative or complementary approach to restore lost vestibular function. At present, the mechanisms underlying hair cell survival and repair are poorly understood, and whether this repair mechanism declines with age is unclear. Our model and data should provide a framework for future studies to interrogate the mechanisms of mammalian hair cell repair.

Methods

Animals. The following mouse strains were used: *Atoh1-CreERTM*, a gift from S. Baker, St. Jude's Hospital, Memphis, TN (31), *Rosa26-tdTomato* (The Jackson Laboratory, stock 007908) (32), *Pou4f3-DTR* (The Jackson Laboratory, stock 028673) (7), and *Plp1-CreERT* (The Jackson Laboratory, stock 5975) (63). Mice of both sexes were used. To induce Cre-recombinase activity for fate mapping, $Atoh1^{CreERTM/+}$; $Rosa26^{tdTomato/+}$ mice were injected with tamoxifen (intraperitoneally, 0.075 mg/g dissolved in corn oil; Sigma) at P1. To selectively ablate hair cells, mice carrying the *Pou4f3-DTR* allele were treated with DT at P1 (intramuscularly, 4 ng/g) immediately prior to tamoxifen injection. For $Pou4f3^{DTR/+}$; $Plp1^{CreERT/+}$; $Rosa26R^{tdTomato/+}$, DT was administered at P1 (intramuscularly, 4 ng/g) to ablate hair cells followed by tamoxifen injection at P8 (intraperitoneally, 0.075 mg/g dissolved in corn oil) for Cre activation (11). Mice were housed in the Stanford University Veterinary Service Center that is fully accredited by the Association for Accreditation and Assessment of Laboratory Animal Care. Food and water were available ad libitum. The mouse room was maintained on a 12-h light/12-h dark cycle in a quiet room. All protocols were approved by the Animal Care and Use Committee of the Stanford University School of Medicine (18606).

Vestibular Physiology, Genotyping, Immunohistochemistry, Image Analysis, and Statistics. See *SI Appendix* for details.

Data Availability. All study data are included in the article and/or *SI Appendix*.

ACKNOWLEDGMENTS. We thank our laboratory members for insightful comments and fruitful discussion on the manuscript; D. Hosseini, P. Vandris, and W. Dong for excellent technical support; S. Baker for sharing the *Atoh1-CreTM* mice; E. Rubel for sharing the *Pou4f3-DTR* mice; and H. Bellen for the Gfi1 antibody. This work was supported by the following grants: American Academy of Otolaryngology–Head and Neck Surgery Resident Centralized Otolaryngology Research Efforts and NIH Loan Repayment Program 2674-9 (to G.S.K.), NIH/National Institute on Deafness and Other Communication Disorders (NIDCD) R21 DC015879 (to T.W.), the Stanford Medical Scholars Research Program, the Howard Hughes Medical Institute Medical Fellows Program, the Stanford Medical Scientist Training Program, NIH/NIDCD F30DC015698 (to Z.N.S.), R01DC016919, R01DC01910, and T32DC015209, and California Initiative in Regenerative Medicine DISC2-10537 (to A.G.C.).

1. A. J. Hudspeth, How the ear's works work. *Nature* **341**, 397–404 (1989).
2. J. Ashmore, J. Gale, The cochlea. *Curr. Biol.* **10**, R325–R327 (2000).
3. O. Bermingham-McDonogh, T. A. Reh, Regulated reprogramming in the regeneration of sensory receptor cells. *Neuron* **71**, 389–405 (2011).
4. J. C. Burns, B. C. Cox, B. R. Thiede, J. Zuo, J. T. Corwin, In vivo proliferative regeneration of balance hair cells in newborn mice. *J. Neurosci.* **32**, 6570–6577 (2012).
5. A. Forge, L. Li, J. T. Corwin, G. Nevill, Ultrastructural evidence for hair cell regeneration in the mammalian inner ear. *Science* **259**, 1616–1619 (1993).
6. A. Forge, L. Li, G. Nevill, Hair cell recovery in the vestibular sensory epithelia of mature guinea pigs. *J. Comp. Neurol.* **397**, 69–88 (1998).
7. J. S. Golub *et al.*, Hair cell replacement in adult mouse utricles after targeted ablation of hair cells with diphtheria toxin. *J. Neurosci.* **32**, 15093–15105 (2012).
8. E. W. Rubel, L. A. Dew, D. W. Roberson, Mammalian vestibular hair cell regeneration. *Science* **267**, 701–707 (1995).
9. T. Wang *et al.*, $Lgr5^{+}$ cells regenerate hair cells via proliferation and direct transdifferentiation in damaged neonatal mouse utricle. *Nat. Commun.* **6**, 6613 (2015).
10. M. E. Warchol, P. R. Lambert, B. J. Goldstein, A. Forge, J. T. Corwin, Regenerative proliferation in inner ear sensory epithelia from adult guinea pigs and humans. *Science* **259**, 1619–1622 (1993).
11. T. Wang *et al.*, Uncoordinated maturation of developing and regenerating postnatal mammalian vestibular hair cells. *PLoS Biol.* **17**, e3000326 (2019).
12. Z. N. Sayyid, T. Wang, L. Chen, S. M. Jones, A. G. Cheng, Atoh1 directs regeneration and functional recovery of the mature mouse vestibular system. *Cell Rep.* **28**, 312–324.e4 (2019).
13. C. Schlecker *et al.*, Selective atonal gene delivery improves balance function in a mouse model of vestibular disease. *Gene Ther.* **18**, 884–890 (2011).
14. Ö. Hızlı *et al.*, Quantitative vestibular labyrinthine otopathology in temporal bones with vestibular schwannoma. *Otolaryngol. Head Neck Surg.* **154**, 150–156 (2016).
15. S. Kariya *et al.*, Histopathologic findings in peripheral vestibular system from patients with systemic lupus erythematosus: A human temporal bone study. *Otol. Neurotol.* **36**, 1702–1707 (2015).
16. J. O. Pickles, M. P. Osborne, S. D. Comis, Vulnerability of tip links between stereocilia to acoustic trauma in the guinea pig. *Hear. Res.* **25**, 173–183 (1987).
17. Y. Zhao, E. N. Yamoah, P. G. Gillespie, Regeneration of broken tip links and restoration of mechanical transduction in hair cells. *Proc. Natl. Acad. Sci. U.S.A.* **93**, 15469–15474 (1996).
18. J. M. Husbands, S. A. Steinberg, R. Kurian, J. C. Saunders, Tip-link integrity on chick tall hair cell stereocilia following intense sound exposure. *Hear. Res.* **135**, 135–145 (1999).
19. S. Jia, S. Yang, W. Guo, D. Z. He, Fate of mammalian cochlear hair cells and stereocilia after loss of the stereocilia. *J. Neurosci.* **29**, 15277–15285 (2009).
20. J. E. Gale, J. R. Meyers, A. Periasamy, J. T. Corwin, Survival of bundleless hair cells and subsequent bundle replacement in the bullfrog's saccule. *J. Neurobiol.* **50**, 81–92 (2002).
21. J. L. Zheng, G. Keller, W. Q. Gao, Immunocytochemical and morphological evidence for intracellular self-repair as an important contributor to mammalian hair cell recovery. *J. Neurosci.* **19**, 2161–2170 (1999).
22. A. Rüsch, R. A. Eatock, A delayed rectifier conductance in type I hair cells of the mouse utricle. *J. Neurophysiol.* **76**, 995–1004 (1996).
23. S. McInturff, J. C. Burns, M. W. Kelley, Characterization of spatial and temporal development of type I and type II hair cells in the mouse utricle using new cell-type-specific markers. *Biol. Open* **7**, bio038083 (2018).
24. G. S. Géléoc, J. R. Holt, Developmental acquisition of sensory transduction in hair cells of the mouse inner ear. *Nat. Neurosci.* **6**, 1019–1020 (2003).
25. M. J. Correia, D. G. Lang, An electrophysiological comparison of solitary type I and type II vestibular hair cells. *Neurosci. Lett.* **116**, 106–111 (1990).
26. R. Geng *et al.*, Usher syndrome IIIA gene clarin-1 is essential for hair cell function and associated neural activation. *Hum. Mol. Genet.* **18**, 2748–2760 (2009).
27. J. F. Krey *et al.*, Plastin 1 widens stereocilia by transforming actin filament packing from hexagonal to liquid. *J. Cell Biol.* **215**, 467–482 (2016).
28. K. Ono *et al.*, Retinoic acid degradation shapes zonal development of vestibular organs and sensitivity to transient linear accelerations. *Nat. Commun.* **11**, 63 (2020).
29. S. A. Bucks *et al.*, Supporting cells remove and replace sensory receptor hair cells in a balance organ of adult mice. *eLife* **6**, e18128 (2017).
30. K. Kawamoto, M. Izumikawa, L. A. Beyer, G. M. Atkin, Y. Raphael, Spontaneous hair cell regeneration in the mouse utricle following gentamicin ototoxicity. *Hear. Res.* **247**, 17–26 (2009).
31. L. M. Chow *et al.*, Inducible Cre recombinase activity in mouse cerebellar granule cell precursors and inner ear hair cells. *Dev. Dyn.* **235**, 2991–2998 (2006).
32. L. Madisen *et al.*, A robust and high-throughput Cre reporting and characterization system for the whole mouse brain. *Nat. Neurosci.* **13**, 133–140 (2010).
33. J. C. Burns, D. On, W. Baker, M. S. Collado, J. T. Corwin, Over half the hair cells in the mouse utricle first appear after birth, with significant numbers originating from early postnatal mitotic production in peripheral and striolar growth zones. *J. Assoc. Res. Otolaryngol.* **13**, 609–627 (2012).
34. L. Tong *et al.*, Selective deletion of cochlear hair cells causes rapid age-dependent changes in spiral ganglion and cochlear nucleus neurons. *J. Neurosci.* **35**, 7878–7891 (2015).
35. T. A. Jones, S. M. Jones, Short latency compound action potentials from mammalian gravity receptor organs. *Hear. Res.* **136**, 75–85 (1999).
36. A. Lysakowski, J. M. Goldberg, A regional ultrastructural analysis of the cellular and synaptic architecture in the chinchilla cristae ampullares. *J. Comp. Neurol.* **389**, 419–443 (1997).
37. R. Pujol, S. B. Pickett, T. B. Nguyen, J. S. Stone, Large basolateral processes on type II hair cells are novel processing units in mammalian vestibular organs. *J. Comp. Neurol.* **522**, 3141–3159 (2014).
38. A. Rüsch, A. Lysakowski, R. A. Eatock, Postnatal development of type I and type II hair cells in the mouse utricle: Acquisition of voltage-gated conductances and differentiated morphology. *J. Neurosci.* **18**, 7487–7501 (1998).
39. M. E. Warchol, R. Massoodnia, R. Pujol, B. C. Cox, J. S. Stone, Development of hair cell phenotype and calyx nerve terminals in the neonatal mouse utricle. *J. Comp. Neurol.* **527**, 1913–1928 (2019).
40. M. E. Warchol, J. D. Speck, Expression of GATA3 and tenascin in the avian vestibular maculae: Normative patterns and changes during sensory regeneration. *J. Comp. Neurol.* **500**, 646–657 (2007).
41. A. Lysakowski *et al.*, Molecular microdomains in a sensory terminal, the vestibular calyx ending. *J. Neurosci.* **31**, 10101–10114 (2011).
42. D. J. Swartz, P. A. Santi, Immunolocalization of tenascin in the chinchilla inner ear. *Hear. Res.* **130**, 108–114 (1999).
43. N. Schug *et al.*, Differential expression of otoferlin in brain, vestibular system, immature and mature cochlea of the rat. *Eur. J. Neurosci.* **24**, 3372–3380 (2006).
44. B. Xiao *et al.*, Homer regulates the association of group 1 metabotropic glutamate receptors with multivalent complexes of Homer-related, synaptic proteins. *Neuron* **21**, 707–716 (1998).

45. B. Xiao, J. C. Tu, P. F. Worley, Homer: A link between neural activity and glutamate receptor function. *Curr. Opin. Neurobiol.* **10**, 370–374 (2000).
46. T. T. Hickman, K. Hashimoto, L. D. Liberman, M. C. Liberman, Synaptic migration and reorganization after noise exposure suggests regeneration in a mature mammalian cochlea. *Sci. Rep.* **10**, 19945 (2020).
47. P. J. Atkinson, E. Huarcaya Najarro, Z. N. Sayyid, A. G. Cheng, Sensory hair cell development and regeneration: Similarities and differences. *Development* **142**, 1561–1571 (2015).
48. S. Raft *et al.*, Cross-regulation of Ngn1 and Math1 coordinates the production of neurons and sensory hair cells during inner ear development. *Development* **134**, 4405–4415 (2007).
49. K. Denman-Johnson, A. Forge, Establishment of hair bundle polarity and orientation in the developing vestibular system of the mouse. *J. Neurocytol.* **28**, 821–835 (1999).
50. J. P. Mbiene, D. Favre, A. Sans, The pattern of ciliary development in fetal mouse vestibular receptors. A qualitative and quantitative SEM study. *Anat. Embryol. (Berl.)* **170**, 229–238 (1984).
51. B. J. Dye, T. C. Frank, S. D. Newlands, J. D. Dickman, Distribution and time course of hair cell regeneration in the pigeon utricle. *Hear. Res.* **133**, 17–26 (1999).
52. T. C. Frank, B. J. Dye, S. D. Newlands, J. D. Dickman, Streptomycin ototoxicity and hair cell regeneration in the adult pigeon utricle. *Laryngoscope* **109**, 356–361 (1999).
53. M. Zakir, J. D. Dickman, Regeneration of vestibular otolith afferents after ototoxic damage. *J. Neurosci.* **26**, 2881–2893 (2006).
54. R. Boyle, S. M. Highstein, J. P. Carey, J. Xu, Functional recovery of anterior semicircular canal afferents following hair cell regeneration in birds. *J. Assoc. Res. Otolaryngol.* **3**, 149–166 (2002).
55. A. Haque, M. Zakir, J. D. Dickman, Recovery of gaze stability during vestibular regeneration. *J. Neurophysiol.* **99**, 853–865 (2008).
56. W. Li, M. J. Correia, Recovery of semicircular canal primary afferent activity in the pigeon after streptomycin ototoxicity. *J. Neurophysiol.* **80**, 3297–3311 (1998).
57. D. R. Sultemeier, L. F. Hoffman, Partial aminoglycoside lesions in vestibular epithelia reveal broad sensory dysfunction associated with modest hair cell loss and afferent calyx retraction. *Front. Cell. Neurosci.* **11**, 331 (2017).
58. H. P. Erickson, M. A. Bourdon, Tenascin: An extracellular matrix protein prominent in specialized embryonic tissues and tumors. *Annu. Rev. Cell Biol.* **5**, 71–92 (1989).
59. T. Sakakura, I. Kusano, Tenascin in tissue perturbation repair. *Acta Pathol. Jpn.* **41**, 247–258 (1991).
60. P. C. Yu, J. L. Du, Transient receptor potential canonical channels in angiogenesis and axon guidance. *Cell. Mol. Life Sci.* **68**, 3815–3821 (2011).
61. A. M. Nazareth, T. A. Jones, Central and peripheral components of short latency vestibular responses in the chicken. *J. Vestib. Res.* **8**, 233–252 (1998).
62. J. F. Krey *et al.*, Annexin A5 is the most abundant membrane-associated protein in stereocilia but is dispensable for hair-bundle development and function. *Sci. Rep.* **6**, 27221 (2016).
63. N. H. Doerflinger, W. B. Macklin, B. Popko, Inducible site-specific recombination in myelinating cells. *Genesis* **35**, 63–72 (2003).